Distinguishing polymeric insulators PD sources through RF PD measurement

Ali Abedini-Livari[1], Keyvan Firuzi[1], Mehdi Vakilian[1] ✉

[1]*Electrical Engineering Department and Centre of Excellence in Power System Management and Control, Sharif University of Technology, Tehran, Iran*
✉ *E-mail: vakilian@sharif.ir*

Abstract: A better performance and consequently the widespread use of polymeric insulators in different parts of the power grid can increase their role in the grid reliability. The accumulation of contamination and housing-erosion are the two most effective factors in undermining the performance of this type of insulators. Therefore, electric utilities need to identify contaminated insulators for washing and cracks in polymeric housing to replace them with healthy specimens. This paper discusses the impact of contamination layer and housing-erosion of polymeric insulators on the partial discharges (PD) at the insulator surface, through RF-PRPD (phase resolved partial discharge) patterns. The existence of different sources of PDs in a real environment (transmission line or station) makes it difficult to use the PRPD patterns to distinguish them from each other. Therefore, using a conical monopole antenna, the simultaneous PD signals and the related RF-PRPD pattern of samples under test are captured. The grayscale image was obtained using the time-frequency matrix of the PD signals transform, by wavelet. Then, features are extracted and selected from grayscale image. By clustering of the PD signals, the resulted RF-PRPD sub-patterns are well separated and provided the necessary means to distinguish among the status of different samples under test.

1 Introduction

Power system transmission and distribution insulators are one of the most effective equipment in the reliability of the power grid. In recent years, the use of polymeric insulators has become commonplace due to better performance in the humid and contaminated conditions [1].

Hydrophobicity is one of the essential and practical properties of polymeric insulators. This feature prevents the insulator surface from being completely covered with water in humid and rainy conditions. As a result, the flashover voltage of the insulator does not decrease too much [2].

Ageing and pollution level are two factors that cause polymeric insulators to malfunction. Dissolving contaminants accumulated at the surface of the insulator in rainwater increases the surface conductivity of the insulator, as a result, the leakage current passing through the insulation surface increases. The thermal energy produced as a result of leakage current causes the water layer to evaporate at some points on the surface of the polymeric insulator. The uneven distribution of the electric field at the insulator surface and its increase in the dry bands cause partial discharges (PDs) at the insulation surface. The growth of the PDs at the surface of the insulator causes a flashover [3]. To avoid these problems, electric utilities need to identify polluted insulators to wash them.

As a result of ageing, the hydrophobicity of the polymeric insulator is reduced. This causes the surface of the polymeric insulator to be utterly wet in humid conditions, reducing the flashover voltage of insulator and reliability of operation [4]. Environmental factors and electrical stresses cause the ageing of the polymeric insulators [5]. In [6], the effect of the thickness and conductivity of the pollution layer accumulated on the polymeric insulation surface which is located inside an electric field distribution has been demonstrated. The results show that by increasing the conductivity and thickness of the pollution layer, the electrical stresses increase along the insulator. As the insulator ages and the contamination level on the surface increases, PD activities increase [7]. The occurrence of PD at the insulation surface is one of the causes of polymer chain degradation, resulting in the ageing of the polymeric insulator [8, 9]. The influence of relative humidity, ageing and contamination level on PRPD patterns of PD activities on the polymeric insulator is discussed in [3]. The results show the ascending trend of the peak value and number of PDs with increasing relative humidity and contamination level. The presence of pollution at the insulation surface changes the PRPD patterns. These patterns can be used to identify the contamination level of a polymeric insulator [10]. To avoid intensifying the process of ageing of the polymeric insulator, contaminated insulators should be identified and washed.

In some cases, with the ageing of the polymeric insulator, erosions and cracks are observed in the polymeric housing of the Fibre Glass Reinforced (FRP) rod [11, 12]. The presence of defects like deep housing-erosion changes the distribution of the electric field and increases its value along with defected insulator relative to the healthy insulator. These erosions occur mostly at the end fittings and cause the more ageing of the insulator by increasing electrical stress [13]. Fahimi *et al.* [14] examine the process of changing the third and fifth harmonics of leakage current during 15 days of testing the defected insulators. The results showed the decreasing trend; for the defected insulator and the increasing trend; for the healthy sample. Exposure of FRP core to the environmental and electrical stresses causes the tracking and cracks on it and reduces the mechanical strength of insulator. Given these reasons, these defective insulators should be detected and replaced with new and healthy ones [12–15].

The financial constraints of the electric utilities make them more willing to make the maximum advantage out of the equipment available in the power grid. Owing to the fact that polymeric insulators are widely used in the power grid, it is important to determine the status of insulators in deciding whether to wash or replace them because of contamination or defects like housing-erosion. PD signals are used to detect the type of defects in other power equipment insulation and their location, such as transformer [16, 17], therefore authors believe a high potential exists that these signals can be used in the detection of types of faults in polymeric insulators. Also, due to the different sources of PD activities in the real environment, it is important to separate PD signals from different sources to decide on the type of defects in the equipment insulation system. Firuzi *et al.* [18] used the DBSCAN clustering method to discriminate multi-source PD
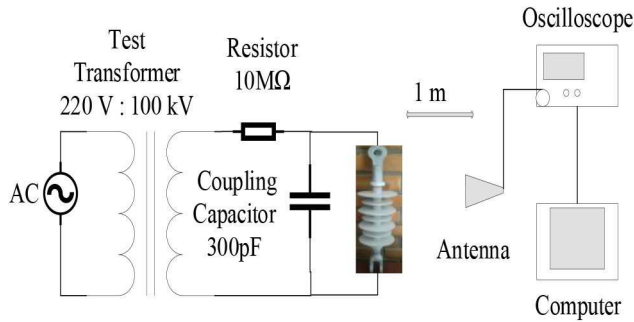
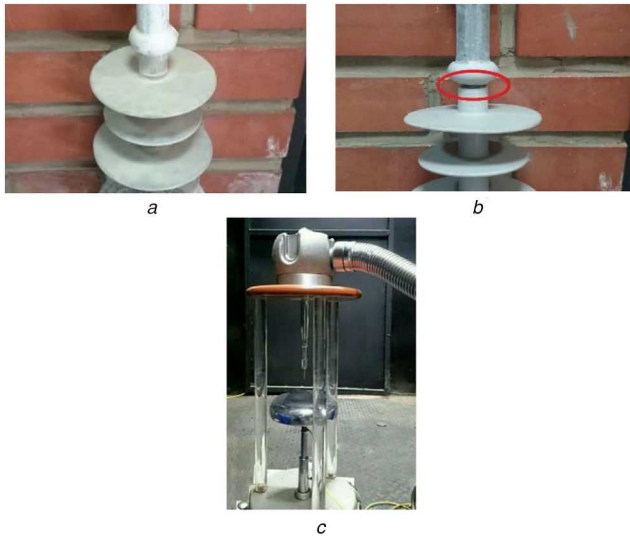**Fig. 1** *Schematic diagram of setup used to measure PD signals*

Fig. 2 *Simulated test samples*
(a) Contaminated sample, *(b)* Deep housing-erosion of the FRP rod, *(c)* Pin-plate configuration (corona PD source)

signals. Anjum *et al*. [19] has shown the use of PD signals to detect the defective discs in ceramic insulators to replace them with new ones. Electromagnetic waves caused by PD activities on insulators in urban areas interfere with radio waves. Moore *et al*. [20] identify the three-dimensional position of the PDs that occur on the defective insulators of 132 kV overhead lines in order to prevent their interference with radio and television receptions. The use of PRPD patterns and PD signals at the same time is useful to detect defects in the insulation of electrical equipment [21].

The rest of this paper is divided into the following sections: in Section 2, test setup and test samples are described. In Section 3, the histogram of oriented gradients (HOGs) feature extraction method by the use of greyscale image obtained from wavelet transform matrix of the PD signals and the reduction of feature space dimensions by the principal component analysis (PCA) method are described. Section 4 describes the Davies–Bouldin criterion and *k*-medoids method to determine the number of PD sources and the employed clustering method. In Section 5, PD signals and radiofrequency (RF)-PRPD patterns due to the pollution layer and housing-erosion of FRP rod are investigated. Considering the concurrent occurrence of these defects and formation of pollution layer on insulators surfaces, simultaneously in the field, the RF-PRPD pattern and PD signals of the healthy insulator, insulator with deep housing-erosion, an insulator with the polluted surface and the corona discharge (as a common discharge in a real environment) are recorded simultaneously. Using the feature extraction and clustering methods described, the RF-PRPD sub-patterns of healthy, polluted and defected insulators are separated to determine the status of different samples.

2 Test setup

The test circuit consists of 50 Hz, 5 kVA, 100 kV test transformer, 300 pF coupling capacitor and 10 MΩ current-limiting resistor. The

conical monopole antenna connected to a 1 GHz oscilloscope with a sampling rate of 5 GSa/s is used to detect PD signals as shown in Fig. 1. In this study, 20 kV polymeric insulator S7 series manufactured by Niroo Kelid Pars Co. was used [22].

The contamination on the surface of the polymeric insulator changes the patterns of PRPD [10]. ESDD and NSDD information of 12 insulators from the Hormozgan province (in the south of Iran) are used to simulate the pollution layer of the contaminated specimen. Most insulators had a 'very heavy' pollution level with a mean conductivity of 0.0307 S/m dissolved in 1 L distilled water [23]. Insulators with this contamination level must be identified and washed to prevent them from malfunctioning. A contaminated sample is simulated using 36 g of kaolin and 28 g of salt dissolved in 1 L of distilled water with the conductivity of 0.0307 S/m and spraying it on the specimen as shown in Fig. 2*a* [24].

The FRP rod of the insulator is responsible for its mechanical strength. One of the reasons for the mechanical failure of the polymeric insulators is the brittle fracture of FRP rod, which is often seen at the energised end fitting [15]. Since the polymeric housing of the rod is responsible for protecting it against environmental destructive factors, any deep erosion of the polymeric housing of the FRP rod in this area, as a result of ageing, increases the probability of mechanical failure of insulators [12]. Examination of specimens with different lengths and shapes of housing-erosion showed that these erosion parameters had the greatest effect on the amplitude of PDs, while slight differences in the RF-PRPD patterns of them were found. As shown in Fig. 2*b*, a deep housing-erosion was discovered on the sample under study which demonstrated the effect of erosion on the measured PD signals.

Corona is one of the common PD sources in power transmission and distribution lines and substations. The pin-plate configuration is used to simulate the corona discharges as shown in Fig. 2*c*.

The sampling rate of the oscilloscope is 2 GS/s. The PD signals and their occurrence phases are recorded and stored over 3.5 μs time intervals. Therefore, each of these PD signal samples consists of 7000 points.

3 Feature extraction

The feature extraction and clustering of PD signals are used to distinguish PD sources. To reduce the effect of the distance between the antenna and the insulators, each PD signal is normalised to its maximum absolute value. The wavelet transform and the HOGs feature extraction method are used to distinguish the PD signals from the different samples.

3.1 Wavelet transform

The features extracted from the time–frequency transforms of PD signals have an excellent ability to distinguish different sources of these signals from one another [21]. Wavelet transforms are popular because the transformed signal contains both time and frequency information [25]. Wavelet transform of a signal can be described as

$$\mathrm{CWT}_x^\Psi(\tau, s) = \frac{1}{\sqrt{|s|}} \int_{-\square}^{+\square} X(t)\psi_{\tau,s}^*(t)\, \mathrm{d}t$$
$$\Psi_{\tau,s} = \frac{1}{\sqrt{|s|}}\psi\!\left(\frac{t-\tau}{s}\right) \tag{1}$$

where $X(t)$, $\psi(t)$, s and τ are normalised PD signal, mother wavelet, scaling factor and shift factor, respectively.

In this paper, generalised Morse wavelets are used to transform PD signals [26]. Magnitude scalogram of the wavelet transform of a sample PD signal is shown in Fig. 3*a*. Given that the output of the analytic wavelets is complex, the magnitude of each element in the wavelet transform matrix is calculated. Depending on the size of the PD signals, the greyscale image size will be 99×7000 pixels.
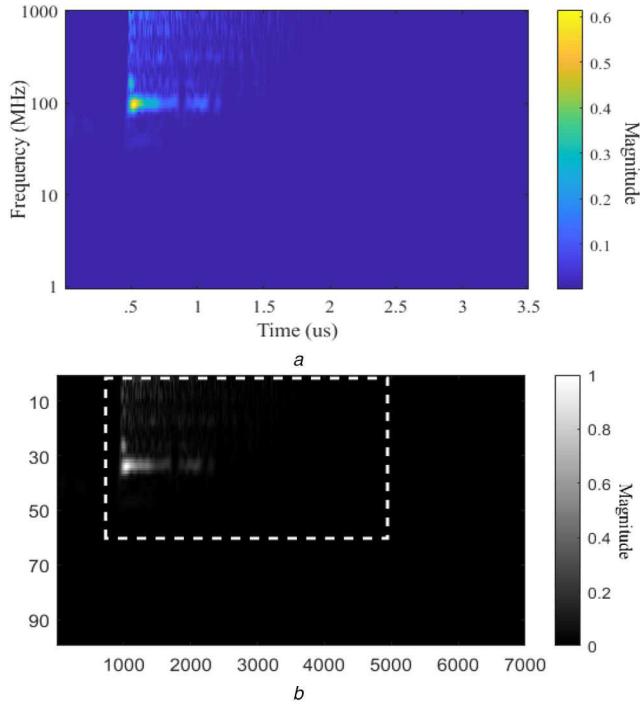
Fig. 3 *Greyscale image*
(a) Magnitude scalogram of the wavelet transform of PD signal, *(b)* Greyscale image and selected part to extract HOG features
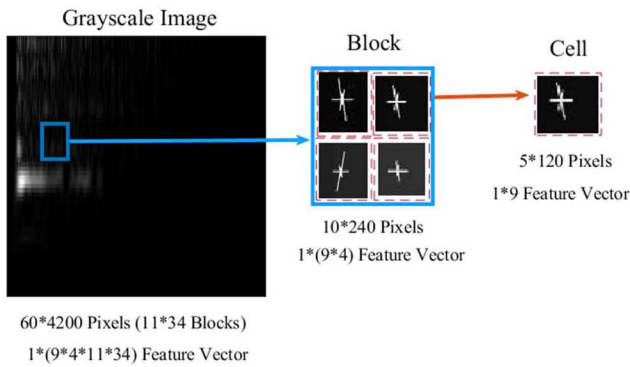

Fig. 4 *HOG feature extraction method*

3.2 Greyscale image

To avoid any information loss, the extracted greyscale image from the wavelet transform of the PD signals is used to extract features. By converting the elements of wavelet transform matrix (I) to values between zero and one, the corresponding greyscale image (s) is obtained (see (2))

$$S_{i,j} = \frac{I_{i,j} - \min(I)}{\max(I) - \min(I)} \qquad (2)$$

where $\max(I)$ and $\min(I)$ are maximum and minimum values of the matrix I elements. As shown in Fig. 3*b*, to reduce the input data, a smaller part of the image containing useful data is used for feature extraction (60×4200 pixels).

3.3 Histogram of oriented gradients

HOGs is a feature extraction method from an image that is mostly used for identifying objects in the computer vision field. The analysis of the greyscale image is performed to extract the features based on the HOG method [27, 28]. First, the image is divided into cells which consist of 5×120 pixels (so each image is made up of 12×35 cells). Magnitude and orientation of gradient values in polar coordinates (M and θ) for each pixel $[i, j]$ of cells are computed and put in bins (see (3)). Nine orientation bins that are

uniformly distributed over 0°–180° are used. All magnitude of the gradients (M) of pixels in a cell for each orientation is added together to form the feature vector of a cell. So, the size of the feature vector for each cell will be 1×9

$$
\begin{aligned}
M(i, j) &= \sqrt{M_x^2(i, j) + M_y^2(i, j)} \\
\theta(i, j) &= \tan^{-1}(M_y(i, j)/M_x(i, j)) \\
M_x(i, j) &= M(i + 1, j) - M(i - 1, j) \\
M_y(i, j) &= M(i, j + 1) - M(i, j - 1)
\end{aligned}
\qquad (3)
$$

Every four adjacent cells form a block. So the size of the feature vector (V) for each block is 1×36. This feature vector is normalised for each block

$$V_{\text{normalized}}(n) = \frac{v(n)}{\sqrt{1 + \sum_{k=1}^{36} v(k)^2}} \qquad (4)$$

This normalisation is done for all four adjacent blocks, respectively. So at the end of this step, the feature vector will be a $1 \times [(12-1) \times (35-1) \times 36] = 1 \times 13{,}464$ vector for each image as shown in Fig. 4. Due to the high number of features, PCA transform is used to reduce the size of the feature space.

3.4 PCA transform

Due to a high number of extracted features, the resultant feature space is of a high-dimensional characteristic. Many of these features do not help to clearly distinguish the status of tested samples. However, one of the methods to reduce the dimensionality of the feature space is to use the PCA method and select a limited number of the best features that enable us to cluster PD signals emitted from different samples [29].

At first, the covariance matrix (C) of the feature space (F) is calculated

$$C = (C_{ij} | C_{ij} = \text{cov}(F_i, F_j)) \qquad (5)$$

Concerning (6), the eigenvalues (λ) and eigenvectors (x) are obtained

$$
\begin{aligned}
\det(C - \lambda I) &= 0 \\
(C - \lambda I)x &= 0
\end{aligned}
\qquad (6)
$$

The absolute magnitude of the eigenvalue indicates the greater variance of the data along the corresponding eigenvector. Using the PCA, the two features corresponding to eigenvectors that have the biggest eigenvalue and are most capable of distinguishing the PD signals that occurred on different samples are selected.

4 PD source clustering

Clustering by using the extracted features is used to illustrate the distinction among the PD signals originated from different sources.

4.1 K-medoids clustering method

K-medoids is one of the famous data clustering methods. This method is resistant to outlier data. In contrast to the *k*-means method that the centre of the cluster is gravity-based; in this method, the centre of the cluster itself is a member of the cluster [30].

After determining the initial medoids, each data point is placed in the cluster of closest medoid to itself. The sum of the distances of each data point from the medoid points corresponding to its cluster is calculated as

$$S = \sum_{j=1}^{k} \sum_{d_i \in C_j} |d_i - m_j| \qquad (7)$$

In which k is the number of clusters, d_i is data points that belong to cluster j (C_j) and m_j is medoid of cluster j.

If the S-value is reduced by replacing each of the medoids with a non-medoids data point, the new point is considered as the new medoid point. This algorithm repeats until the medoids remain unchanged.

For using this method the number of clusters must be determined. Davies–Bouldin criterion is used to determine the number of clusters.

4.2 Davies–Bouldin criterion

This method first clusters the data using the k-means algorithm for different values of k and then determines the number of clusters by measuring the within-cluster and between-cluster intervals as [31]:

$$\mathrm{DB} = \frac{1}{k}\sum_{i=1}^{k}\max_{j \neq i}\{D_{i,j}\}$$

$$D_{i,j} = \frac{(d_i + d_j)}{d_{i,j}} \qquad (8)$$

$$d_{i,j} = d(v_i, v_j), \quad d_i = \frac{1}{\|c_i\|}\sum_{x \in c_i} d(x, v_i)$$

where k, v_i, $d(x, y)$ and $\|c_i\|$ are the number of clusters, centroid of the cluster c_i, Euclidean distance between x and y and norm of c_i. As the within-cluster distance decreases and the between-cluster distance increases, the data are better clustered. So, the best number of clusters has a minimum Davies–Bouldin index value.

5 Results and discussion

In this section, first, the RF-PRPD patterns of healthy, polluted and defected insulators are examined. Due to the proximity of insulators installed in different parts of the power grid, the measured RF-PRPD pattern is the result of PD activities on all nearby insulators and other PD sources such as corona on other equipment with a very short distance from insulators (for insulators in the substations(. For this reason, it is necessary to separate the RF-PRPD sub-patterns from the RF-PRPD. Therefore, in the following case studies, the results of the proposed method for detecting, clustering and separating PD signals co-occurring on the studied samples are investigated. First, three samples consisting of the healthy insulator, polluted insulator, and corona discharge source were tested simultaneously. Then by adding an insulator with housing-erosion to the above three sets of PD sources, the proposed method is evaluated, when there are four PD sources.

5.1 RF-PRPD-based identification

Corona sample and healthy, polluted and defected insulators were tested separately to see the effect of pollution layer and housing-erosion on the PD signals occurring on the polymeric insulators and RF-PRPD patterns. Despite the effect of changes in the relative humidity on the number and magnitude of PD signals occurring on the insulator, this factor does not have a considerable effect on the PRPD patterns and, consequently, the accuracy of the proposed algorithm [7]. The obtained RF-PRPD patterns for each sample and an example of PD signals that occur on each specimen are shown in Fig. 5 along with their greyscale image obtained from their wavelet transform matrix. The density of PD activity increase as the colour changes from blue to yellow in RF-PRPD patterns.

As it can be seen, The RF-PRPD pattern for each sample differs from the other samples. The most similarity is found between the patterns of the cracked sample and the polluted one. However, the level of PD activities during the voltage transition from zero (change of voltage polarity) is higher in the sample preserving a crack, if compared with the polluted sample. In fact, PD activities in this sample are more affected by the change of voltage polarity than the voltage magnitude. This is more evident when the voltage polarity changes from negative to positive values. Despite the similarity in the PD signals occurring on the insulators, differences are observed in the greyscale images obtained from their wavelet transform matrix. HOG features extracted from these images can
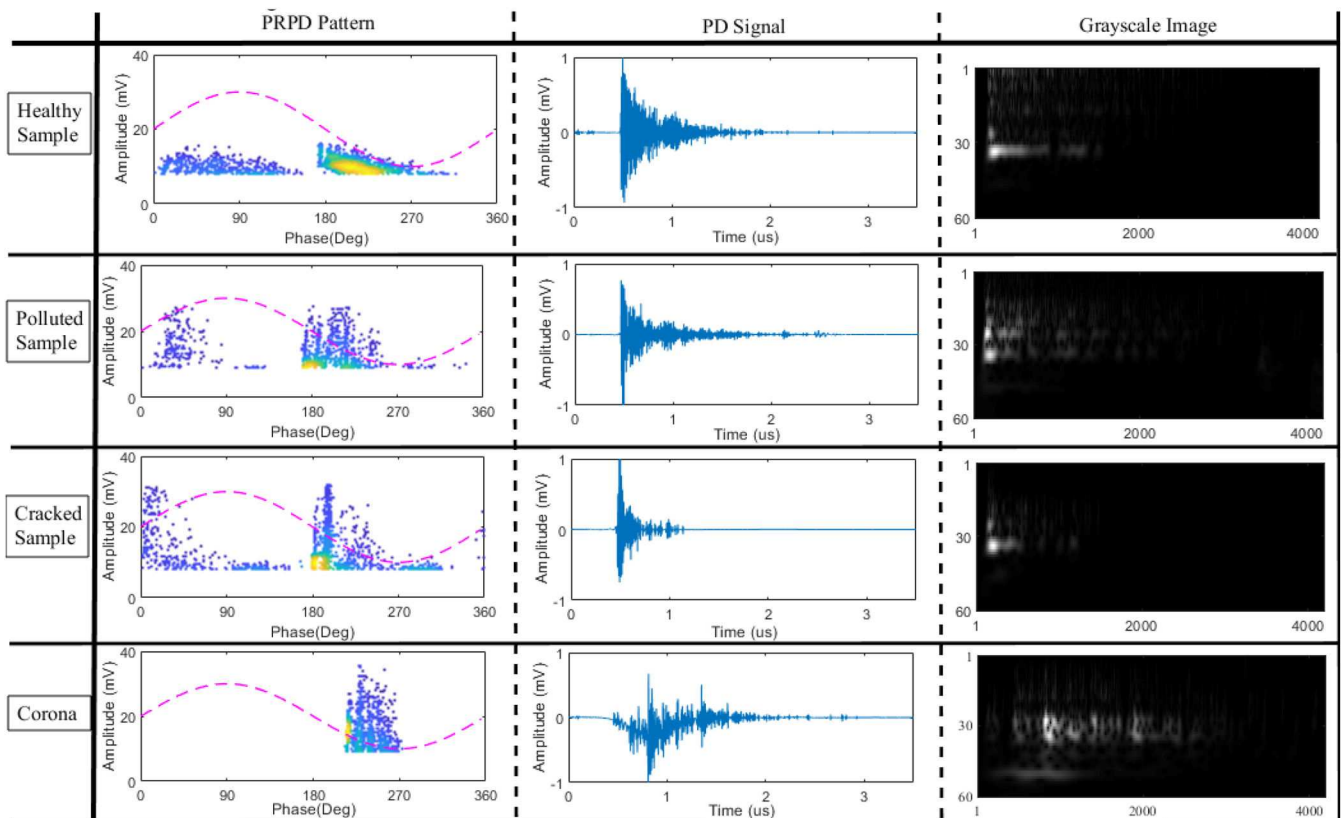

Fig. 5 *Results of testing the samples individually (healthy sample under 54 kV, the polluted sample under 52 kV, the cracked sample under 49 kV, corona under 50 kV)*
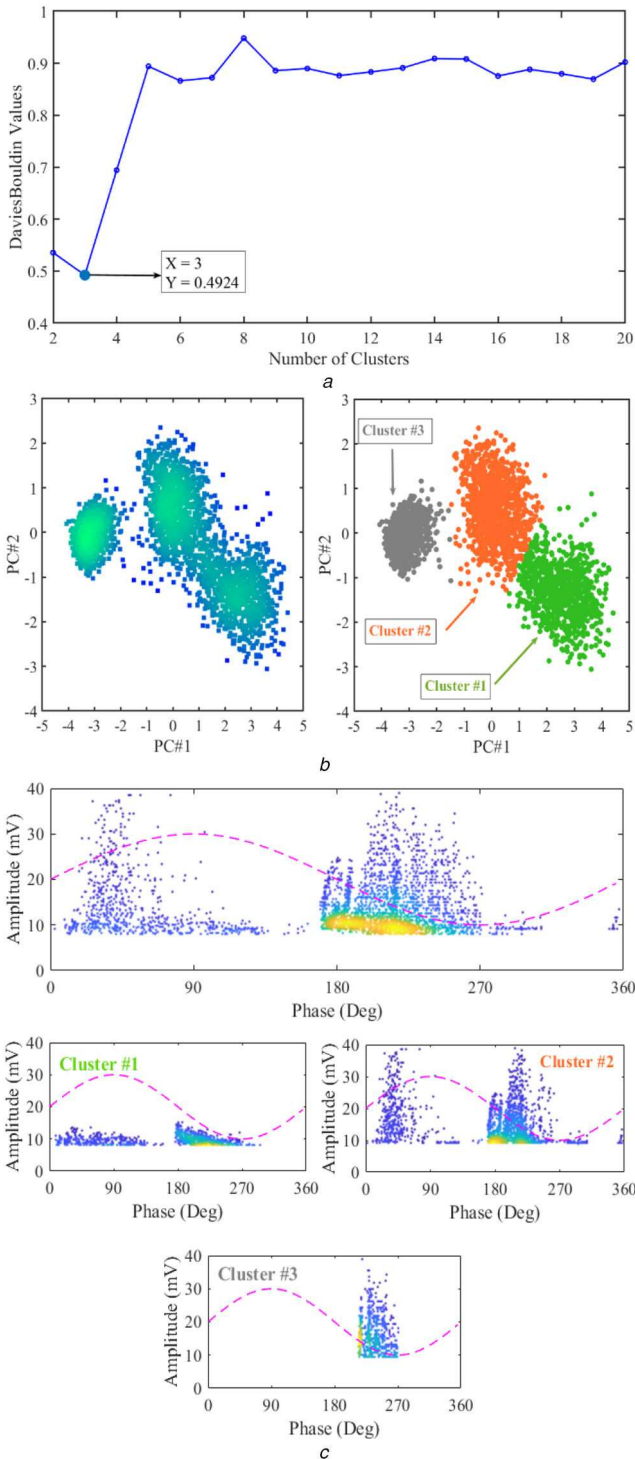*(a)* PRPD patterns, *(b)* PD signal, *(c)* Corresponding greyscale image

Fig. 6 *Distinguishing and identification of polluted insulator*
(a) Davies–Bouldin values (optimal number of clusters), *(b)* *k*-medoids clustering result, *(c)* RF-PRPD and RF-PRPD sub-patterns

be used to cluster different sources of PD signals to elicit RF-PRPD sub-patterns of each insulator from RF-PRPD pattern when they co-occur on the insulators next to each other or there are different sources of PD. Finally, RF-PRPD sub-patterns can be used to identify different sources of PD.

5.2 Distinguishing and identification of polluted insulator

As explained in Section 1, the contamination accumulated at the surface of the polymeric insulators is one of the most important causes of the malfunction of these insulators. Identifying and washing contaminated insulators of power transmission and distribution lines or substations is essential to prevent power outages caused by the malfunction of this component of the power

system. As the shape of the PRPD patterns of the corona and surface PD activities on the polymeric insulators do not change much with changing the level of the applied voltage, the obtained patterns in one voltage level, above the inception voltage of PD, can be used in higher voltage levels as well [10]. In this section, three samples of the healthy insulator, polluted insulator and corona were tested simultaneously at 54 kV, which is equal to the maximum PD inception voltage of all samples. The PDs occurring on samples and their occurrence phase were measured and recorded. According to the proposed method, the HOG feature extraction method was applied to the greyscale images obtained from the wavelet transform matrix of the PD signals. After reducing the size of the feature space and selecting two best features that give the best results in distinguishing among the different specimens using PCA, the number of clusters (PD sources) is determined, using the Davies–Bouldin criterion. As shown in Fig. 6a, this algorithm is well able to calculate the optimal number of clusters in the data (three clusters). For better observation, the clustering results using PC#1 and PC#2 are shown in Fig. 6b. The density of data increase as the colour changes from blue to cyan. Given the ability of the proposed method to distinguish PD signals from different sources, the RF-PRPD sub-patterns corresponding to each sample was elicited from the RF-PRPD pattern obtained from the experiment.

The RF-PRPD pattern and the RF-PRPD sub-patterns are shown in Fig. 6c. Despite the change in test voltage, the RF-PRPD sub-patterns differ slightly from the results in Section 5.1. Considering the similarity of the RF-PRPD sub-patterns obtained in this section with the results shown in Fig. 5, the pattern of each sample is determined. As such, the cluster #1, #2 and #3 are corresponding to the healthy sample, the polluted sample and the corona simulation, respectively.

5.3 Separating polluted and defected insulators

As stated in Section 1, due to the cracks occurring in the polymeric housing of the polymeric insulator, its core is exposed to environmental corrosive materials (such as acid rain). At the same time, PDs occur near the core of the insulator, causing erosion and tracking in FRP core. This factor increases the probability of mechanical failure of insulator. It is challenging to distinguish defected insulator among other insulators with PD activity due to the pollution.

The specimen with housing-erosion was added to the test setup to evaluate the feasibility of the proposed method for separating and identifying contaminated and defected samples. As in the previous section, the PD signals from the samples were recorded simultaneously and then features extracted from them using the wavelet transform, HOG feature extraction method and PCA, respectively. The result of the Davies–Bouldin criterion is shown in Fig. 7a. Given that four clusters has the minimum value of the Davies–Bouldin criterion and it is equal to the number of samples tested, it can be concluded that this algorithm is well able to detect the number of PD sources.

Fig. 7b shows clusters of PD signals from different samples using PC#1 and PC#2. Finally, after clustering, the RF-PRPD sub-patterns are separated. As it can be seen, the first three RF-PRPD sub-patterns are similar to the patterns obtained in the previous section. The fourth sub-pattern is related to the sample added in this section, similar to the pattern shown in Fig. 5 for defected sample, when the sample is tested separately.

As shown in RF-PRPD sub-patterns, more PD activities compared to the PD activities of other samples; when the voltage polarity changes from negative to positive, is an indication of proper pattern recognition for this sample. Finally, using the new approach that introduced in this paper it is possible to separate and identify the defected and polluted insulators.

6 Summary and conclusion

Contamination and housing-erosion are the two major factors contributing to the inadequate electrical and mechanical performance of polymeric insulators. In this paper, the effect of pollution layer accumulation on polymeric insulator and deep
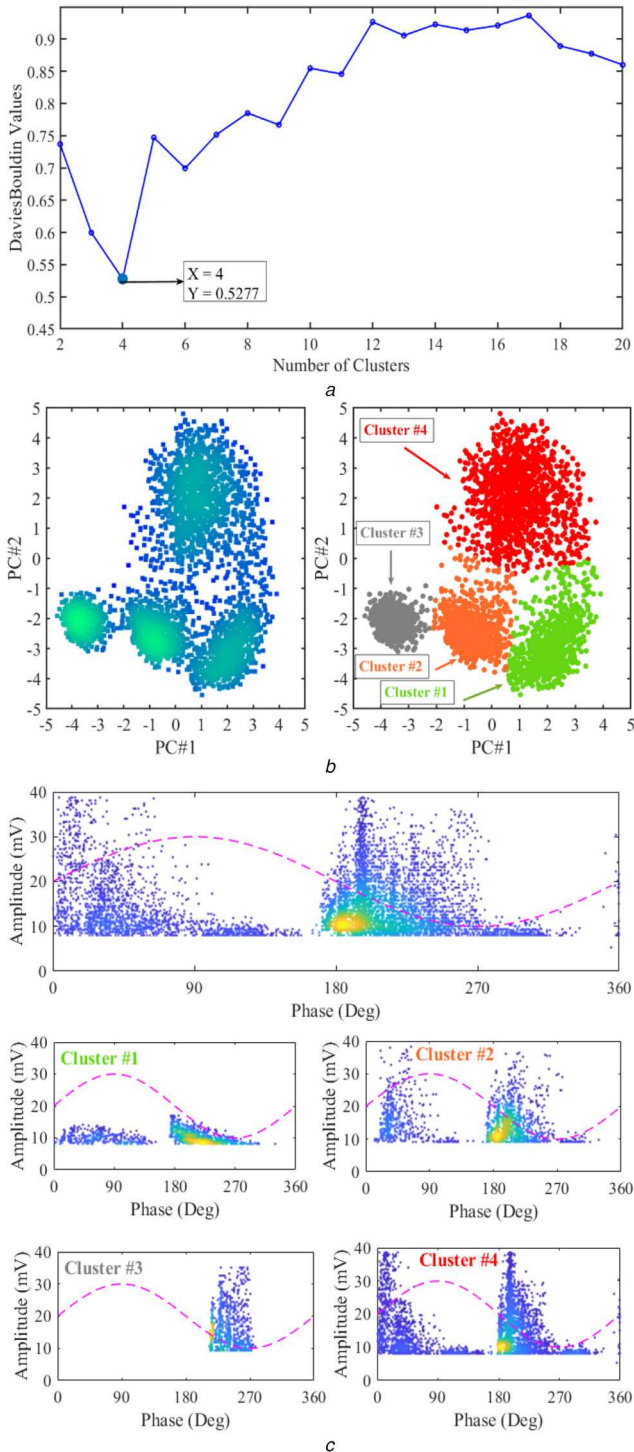
Fig. 7 *Separating polluted and defected insulators*
(a) Davies–Bouldin values (optimal number of clusters), *(b)* k-medoids clustering result, *(c)* RF-PRPD and RF-PRPD sub-patterns

selected. Davies–Bouldin criterion and *k*-medoids method are used to find the number of PD sources and clustering them. Using the clustering results, the PRPD sub-patterns are obtained.

According to the results obtained from the testing of different specimens simultaneously in Sections 5.2 and 5.3 and by using the similarity between the RF-PRPD sub-patterns with the RF-PRPD patterns obtained from testing of each specimen separately, it is verified that the proposed method is capable of distinguishing the healthy insulators, from the insulators that their performance is affected by a high level of pollution on their surface, and those are engaged with a kind of defect (housing erosion). Finally, after determining the status of insulators, it can be decided to wash or replace them in case of excessive contamination, or deep housing-erosion, respectively.

Authors expect that by application of this method, when performing the online PD monitoring and measurement in the field, the PDs that are raised due to insulator surface contamination or a real defect in different parts of a polymeric insulator can be differentiated. Then, based on these results the operating utility can plan its future maintenance and repair work on the lines insulators.

7 References

[1] Mavrikakis, N.C., Mikropoulos, P.N., Siderakis, K.: 'Evaluation of field-ageing effects on insulating materials of composite suspension insulators', *IEEE Trans. Dielectr. Electr. Insul.*, 2017, **24**, (1), pp. 490–498

[2] Haddad, G., Wong, K.L., Petersen, P.: 'Evaluation of the aging process of composite insulator based on surface charaterisation techniques and electrical method', *IEEE Trans. Dielectr. Electr. Insul.*, 2016, **23**, (1), pp. 311–318

[3] Mekala, K., Chandrasekar, S., Ravindra, R.S.: 'Investigations of accelerated aged polymeric insulators using partial discharge signal measurement and analysis', *J. Electr. Eng. Technol.*, 2015, **10**, (1), pp. 299–307

[4] Lan, L., Gorur, R.S.: 'Computation of ac wet flashover voltage of ceramic and composite insulators', *IEEE Trans. Dielectr. Electr. Insul.*, 2008, **15**, (5), pp. 1346–1352

[5] Ahmadi-Joneidi, I., Majzoobi, A., Shayegani-Akmal, A., *et al.*: 'Aging evaluation of silicone rubber insulators using leakage current and flashover voltage analysis', *IEEE Trans. Dielectr. Electr. Insul.*, 2013, **20**, (1), pp. 212–220

[6] Arshad, A., Nekahi, A., McMeekin, S.G., *et al.*: 'Effect of pollution severity on electric field distribution along a polymeric insulator'. IEEE 11th Int. Conf. on the Properties and Applications of Dielectric Materials (ICPADM), Sydney, Australia, 2015, pp. 612–615

[7] Jayaprakash Narayanan, V., Karthik, B., Chandrasekar, S.: 'Flashover prediction of polymeric insulators using PD signal time-frequency analysis and BPA neural network technique', *J. Electr. Eng. Technol.*, 2014, **9**, (4), pp. 1375–1384

[8] Moreno, V.M., Gorur, R.S.: 'Effect of long-term corona on non-ceramic outdoor insulator housing materials', *IEEE Trans. Dielectr. Electr. Insul.*, 2001, **8**, (1), pp. 117–128

[9] Nazir, M.T., Phung, B.T., Hoffman, M.: 'Performance of silicone rubber composites with SiO_2 micro/nano-filler under AC corona discharge', *IEEE Trans. Dielectr. Electr. Insul.*, 2016, **23**, (5), pp. 2804–2815

[10] Saadati, H., Shayegani, A.A., Borsi, H., *et al.*: 'Partial discharge of polymeric insulators under artificial pollution'. 18th Int. Symp. on High Voltage Engineering, Seoul, Republic of Korea, 2013

[11] 'Dealing with deterioration of silicone insulation in critical applications'. Available at https://www.inmr.com/dealing-deterioration-silicone-insulation-critical-applications/, March 2018

[12] Pinnangudi, B., Gorur, R.S., Poweleit, C.D.: 'Degradation dynamics of polymeric housing materials used for HV line and station apparatus', *IEEE Trans. Dielectr. Electr. Insul.*, 2007, **14**, (5), pp. 1215–1222

[13] Vaillancourt, G.H., Carignan, S., Jean, C.: 'Experience with the detection of faulty composite insulators on high-voltage power lines by the electric field measurement method', *IEEE Trans. Power Deliv.*, 1998, **13**, (2), pp. 661–666

[14] Fahimi, N., Chalaki, M.R., Baferani, M.A., *et al.*: 'Investigating the failures of defected silicon rubber insulators in salt-fog hamber', 2018 IEEE Texas Power and Energy Conf. (TPEC), Texas A&M University, USA., 2018, pp. 1–6

[15] Kumosa, M.S., Kumosa, L.S., Armentrout, D.L.: 'Failure analyses of nonceramic insulators part 1: brittle fracture characteristics', *IEEE Electr. Insul. Mag.*, 2005, **21**, (3), pp. 14–27

[16] Firuzi, K., Vakilian, M., Phung, B.T., *et al.*: 'A hybrid transformer PD monitoring method using simultaneous IEC60270 and RF data', *IEEE Trans. Power Deliv.*, 2019, **34**, (4), pp. 1374–1382

[17] Hu, Y., Zeng, Z., Liu, J., *et al.*: 'Design of a distributed UHF sensor array system for PD detection and location in substation', *IEEE Trans. Instrum. Meas.*, 2019, **68**, (6), pp. 1844–1851

[18] Firuzi, K., Vakilian, M.: 'Multi-source partial discharge signals discrimination by six bandpass filters and DBSCAN clustering'. Proc. of IEEE Int. Conf. on Properties and Applications of Dielectric Materials, Xian, People's Republic of China, 2018, vol. 2018-May, pp. 68–71

[19] Anjum, S., Jayaram, S., El-Hag, A., *et al.*: 'Detection and classification of defects in ceramic insulators using RF antenna', *IEEE Trans. Dielectr. Electr. Insul.*, 2017, **24**, (1), pp. 183–190

housing-erosion on PD signals and their resulting RF-PRPD patterns is investigated. Section 5.1 presents PD signals and RF-PRPD patterns obtained from a separate experiment of healthy insulator, polluted insulator, defected insulator and corona sample. Differences in the RF-PRPD patterns can be used to identify the test samples from each other and to plan for washing contaminated specimens and replacing defected insulators.

Given the presence of insulators adjacent to each other in the field conditions, it is important to separate the RF-PRPD sub-patterns from the RF-PRPD pattern to determine the conditions of insulators. HOG features extracted from the greyscale image obtained from the wavelet transform matrix of PD signals were used to cluster different sources of PDs. Using PCA, two features that were most capable of distinguishing among the clusters were

[20] Moore, P.J., Portugués, I.E., Glover, I.A.: 'Remote diagnosis of overhead line insulation defects'. 2004 IEEE Power Engineering Society General Meeting, 2004, vol. 2, pp. 1831–1835

[21] Firuzi, K., Vakilian, M., Darabad, V.P.*, et al.*: 'A novel method for differentiating and clustering multiple partial discharge sources using S transform and bag of words feature', *IEEE Trans. Dielectr. Electr. Insul.*, 2017, **24**, (6), pp. 3694–3702

[22] 'Suspension type insulators- Niroo Kelid Pars co.'. Available at http://nirookelidpars.com/en/suspension-type/

[23] IEC 60815-1: 'Selection and dimensioning of high-voltage insulators for use in polluted conditions', 2008

[24] Abedini-Livari, A., Eshaghi-Maskouni, M., Vakilian, M.*, et al.*: 'Line composite insulators condition monitoring through partial discharge measurement'. 34th Int. Power System Conf., Tehran, Iran, 2019

[25] Lilly, J.M., Olhede, S.C.: 'Generalized Morse wavelets as a superfamily of analytic wavelets', *IEEE Trans. Signal Process.*, 2012, **60**, (11), pp. 6036–6041

[26] Olhede, S.C., Walden, A.T.: 'Generalized Morse wavelets', *IEEE Trans. Signal Process.*, 2002, **50**, (11), pp. 2661–2670

[27] Dalal, N., Triggs, B.: 'Histograms of oriented gradients for human detection'. Proc. – 2005 IEEE Computer Society Conf. on Computer Vision and Pattern Recognition, CVPR 2005, San Diego,CA, USA, 2005, vol. I, pp. 886–893

[28] Firuzi, K., Vakilian, M., Phung, B.T.*, et al.*: 'Partial discharges pattern recognition of transformer defect model by LBP & HOG features', *IEEE Trans. Power Deliv.*, 2019, **34**, (2), pp. 542–550

[29] Picasso, P.: '*Principal component analysis why principal component analysis?*' (Springer, UK, 2002, 2nd edn.)

[30] Kaufman, L., Rousseeuw, P.: '*Finding groups in data: an introduction to cluster analysis*' (John Wiley & Sons, Hoboken, NJ, USA, 2009)

[31] Davies, D.L., Bouldin, D.W.: 'A cluster separation measure', *IEEE Trans. Pattern Anal. Mach. Intell.*, 1979, **PAMI-1**, (2), pp. 224–227

IET Gener. Transm. Distrib., 2020, Vol. 14 Iss. 21, pp. 4859-4865

© The Institution of Engineering and Technology 2020

4865